

IRAS 08544-4431 : a new post-AGB star in a binary system surrounded by a dusty disc. [★]

Thomas Maas¹, Hans Van Winckel^{1**}, Tom Lloyd Evans², Lars-Åke Nyman^{3,4}, Dave Kilkenny⁵, Peter Martinez⁵, Fred Marang⁵, and Francois van Wyk⁵

¹ Instituut voor Sterrenkunde, K.U.Leuven, Celestijnenlaan 200B, B-3001 Leuven, Belgium

² School of Physics and Astronomy, University of St Andrews, North Haugh, St Andrews, Fife, Scotland KY16 9SS

³ European Southern Observatory, Casilla 19001, Santiago 19, Chile

⁴ Onsala Space Observatory, S-43992 Onsala, Sweden

⁵ South African Astronomical Observatory, P. O. Box 9, Observatory 7935, South Africa

Received / Accepted

Abstract. We present an analysis of our extensive data-set on IRAS08544-4431. It is the first object we discuss of our newly defined sample of stars, selected for their position in the ‘RV Tauri’ box in the IRAS [12] – [25], [25] – [60] two-color diagram. Moreover, our selection criteria included an observed excess in the L-band, indicative of a dusty disc. The SED of IRAS08544-4431 shows a broad IR excess starting already at H . Our optical photometric data reveal some evidence for deep and shallow minima in the light curve and a pulsation time-scale of around 100 days with a small amplitude (ΔV peak-to-peak = 0.17 mag). Our CORALIE radial velocity measurements show that IRAS08544-4431 is a binary system with a period of 499 ± 3 days and a mass function of $0.02 M_{\odot}$. Moreover, IRAS08544-4431 is detected in both the CO (2-1) and (1-0) mm-wave emission lines. The triangular shape of the weak CO profile confirms that part of the circumstellar material is not freely expanding but resides probably in a dusty circumbinary disc. Our chemical abundance analysis of a high resolution spectrum of high S/N reveals that a depletion process has modified the photospheric abundances to a moderate extent ($[Zn/Fe]=+0.4$). All these findings confirm that the F-type IRAS08544-4431 is another good example of a binary Post-AGB star surrounded by a dusty disc. The $H\alpha$ P-Cygni profile shows ongoing mass-loss with a very high outflow velocity, the origin of which is not understood. The strength and velocity of the $H\alpha$ -absorption are modulated with the orbital motion; the maxima of both quantities ($\sim 400 \text{ km s}^{-1}$, 5 \AA respectively) occur at superior conjunction.

Key words. stars: abundances - stars: AGB and post-AGB - stars: evolution - stars: individual: IRAS 08544-4431 - stars: individual: RV Tauri - stars: binaries: spectroscopic

1. Introduction

A new set of probable post-AGB stars was found in the IRAS Point Source Catalog by Lloyd Evans (1999 and in preparation). Their recognition follows the finding that the brightest of the RV Tauri stars contained in the General Catalogue of Variable Stars have IRAS photometry which includes a reliable $60 \mu\text{m}$ measurement, so that they may be plotted in a [12] – [25], [25] – [60] two-color diagram. Lloyd Evans (1985) and Raveendran (1989)

remarked on the fact that the region containing these data lies in a well-defined and relatively thinly-populated part of the diagram, which corresponds to the greater relative brightness of these stars at $60 \mu\text{m}$ compared to the majority of the M-type variables which have extensive dust shells. This made feasible a search of the IRAS photometry for new examples of RV Tauri stars, selected by their mid-infrared colors rather than by their variability in blue light. A list of candidates was prepared by calculating the colors of all IRAS stars with reliable (quality 3) photometry at $60 \mu\text{m}$ and selecting those which were located in a rectangle in the IRAS two-color diagram which contained most of the known RV Tauri stars.

The defining rectangle is

$$\begin{cases} [12] - [25] \equiv 1.56 + 2.5 \log[F(25)/F(12)] = 1.0 - 1.55 \\ [25] - [60] \equiv 1.88 + 2.5 \log[F(60)/F(25)] = 0.20 - 1.0 \end{cases}$$

Send offprint requests to: Thomas Maas

^{*} based on observations collected at the European Southern Observatory in Chile (62.L-0508) and at SAAO. The radial velocity data was obtained with the Swiss 1.2m Euler telescope at La Silla, Chile.

^{**} Postdoctoral fellow of the Fund for Scientific Research, Flanders

Correspondence to: Thomas.Maas@ster.kuleuven.ac.be

Table 1. Basic parameters of IRAS 08544 (The coordinates are from the GSC).

IRAS 08544		
Coordinates	α_{2000}	08 56 14.2
	δ_{2000}	-44 43 11.0
Galactic coordinates	l	265.51
	b	+0.39

Over 1000 sources south of 20 deg N declination were located on the Palomar, ESO and/or SRC Sky Survey prints. Those where a reasonably bright star was found were selected for visible-light spectroscopy and near infrared (*JHKL*) photometry. Initial spectroscopic observations made with the Unit Spectrograph and RPCS detector system at the Cassegrain focus of the 1.9m Radcliffe reflector at the Sutherland observing site of the South African Astronomical Observatory covered the approximate range 3500 – 6700 Å, with a resolution of 7 Å. This survey revealed stars of a wide range of spectral types with the excess at L indicative of the presence of a dusty disk (Lloyd Evans 1997). Those objects with spectral types, based primarily on the hydrogen lines in view of the many spectral peculiarities of RV Tauri star spectra, of F, G or K were regarded as possible RV Tauri stars and were selected for additional observations. These included *UBVRI* photometry, of those stars which were not too faint and did not suffer crowding problems, made at Sutherland as part of the SAAO service observing programme.

Repeated near infrared and/or visible light photometry showed that while some of the RV Tauri-like stars are variables of substantial amplitude, most are less variable than typical RV Tauri stars. Lloyd Evans (1999) reported a correlation between amplitude and spectral type: the most variable stars have spectral types in the narrow range occupied by the bulk of the previously-known RV Tauri stars, while those of lesser amplitude are mainly of earlier F subtype. This suggested that many IRAS detected RV Tauri stars of the GCVS are simply those stars with dusty disks which happen to be passing through the instability strip of the Type II Cepheids (Lloyd Evans 1999).

We embarked on monitoring programs both in optical and near-IR photometry at SAAO and radial velocity at La Silla. These data were supplemented with single observations to obtain high-resolution spectroscopy and CO mm-wave line emission. The aim is to characterize these evolved objects, compare them with GCVS RV Tauri stars and to discuss the relationship between the presence of such a disc and the eventual binarity of the central object.

In this first paper devoted to this project, we report on the analysis of an extensive data-set obtained for one object: IRAS 08544-4431 (IRAS 08544 in what follows, see Table 1). It is one of the stars in our sample with a

smaller amplitude and is of spectral type F3, which was determined on the basis of a low resolution spectrum (Lloyd Evans 1999). The object was selected, despite the low quality flag (2) of the 60 μm flux point, because of its LRS spectrum. In the literature this little studied object is referred to as a carbon star following the LRS IRAS spectral classification (Kwok et al. 1997). The LRS spectrum is, however, rather featureless and in this paper we argue that the spectrum is not that of a C-rich object (Olnon et al. 1986) and that the star is certainly not a carbon star. In following papers we will describe the overall characteristics of the sample. In Sect.2 we outline the observational dataset and the reduction procedures, next we discuss the Spectral Energy Distribution (SED). In Sect.4 we show that IRAS 08544 is variable with a small amplitude and long timescale. There is some hint that the defining light curve of GCVS RV Tauri stars is also present in IRAS 08544, but a dedicated monitoring program is needed to study this in more detail. In Sect.5 the radial velocity measurements are presented, proving that IRAS 08544 is a binary; we also used our CORALIE data to study the variation of the P Cygni profile of H α . In Sect. 6 we present our CO line emission measurements and in Sect.7 our chemical abundance analysis shows that depletion, which is a widespread phenomenon among RV Tauri stars, has slightly altered the photospheric abundances of IRAS 08544 as well. In Sect.8 we put our main conclusions together and end with a discussion.

2. Observations

2.1. Photometry

Infrared observations on the *JHKL* system defined by the standard stars of Carter (1990) were made with the Mark II Infrared Photometer on the 0.75 m reflector at Sutherland (SAAO Facilities Manual). *L* has the mean effective wavelength of 3.5 μm and not 3.8 μm for which the same symbol is sometimes used. Standard errors for this bright source are 0.03 mag for *J*, *H* and *K* and 0.05 mag for *L*. Individual observations will be given along with those of other stars by Lloyd Evans (in preparation).

Photometric observations on the *UBVRI* system were made with the Modular Photometer on the 0.5 m telescope at Sutherland on 54 nights from JD 2450858 to 2451666, with repeated observations on several nights. Observations were continued with the 0.75 m Automatic Photoelectric Telescope (APT) (Martinez et al. 2002) on 37 nights from JD 2451929 to 2452060. This concentrated run of observations made with the APT proved invaluable in showing that the pulsation time-scale was of the order of 100 days. The observations were made with reference to the Cousins *UBVRI* standards in the E-regions (Menzies et al. 1989), and reduced to the standard system using color terms derived from observations of standard stars of a wide range of color. There was no local standard star and hence the data include the increased random errors involved in a magnitude transfer through a large angle. The nominal

error of a single observation is typically 0.007 mag but may be substantially larger in $U - B$, especially on bright moonlit nights, to which has to be added the contribution, perhaps of order 0.01 mag, of the E-region transfer.

2.2. Spectroscopy

2.2.1. Low Resolution spectra.

The first spectra were taken with the RPCS detector on the Unit Spectrograph at the Cassegrain focus of the 1.9 m Radcliffe reflector at the Sutherland observatory of the SAAO. Spectra taken over the range 3500-7000 Å with a resolution of 7 Å were classified against a set of MK standard star spectra and a hydrogen-line type of F3 was obtained from the higher Balmer lines (since $H\alpha$ at least is always in emission) in the same way as for a large sample of known RV Tau stars observed earlier with a photographic detector on the same spectrograph. IRAS 08544 is thus one of the stars, described as RV Tau-like on the basis of their spectral energy distribution and F-G spectral type, which lie outside and on the hot side of the instability strip (Lloyd Evans 1999).

2.2.2. FEROS spectrum

A high signal-to-noise and high resolution ($\lambda/\delta\lambda \sim 48000$) spectrum was obtained with FEROS mounted on the 1.52 m ESO telescope at La Silla (Chile). FEROS is a fiber fed echelle spectrograph which covers the complete optical region from 3700 to 8600 Å. The spectrograph is equipped with a CCD camera incorporating a chip with 2048 x 4096 pixels of 15 x 15 μm . The online reduction consists of background subtraction, order extraction, flat-fielding and wavelength calibration, using a Th-Ar spectrum. We normalized the reduced spectra using smoothed splines on interactively determined continuum points. The FEROS spectrum was obtained on January 26th 1999. Sample spectra are shown in Figs. 12 and 13.

2.2.3. CORALIE data

We have been monitoring IRAS08544 with the spectrograph CORALIE mounted on the Swiss telescope at La Silla, ESO Chile. CORALIE (Queloz et al. 1999) is a high resolution ($\lambda/\delta\lambda = 50000$) fiber fed echelle spectrograph which is constructed to perform high precision velocity measurements. Cross-correlation profiles are calculated on-line with a standard F mask. To improve the cross-correlation profiles we constructed a individual mask for IRAS08544 tuned on the basis of the FEROS spectrum. The radial velocities are obtained by Gaussian fitting of these profiles. We started this monitoring in November 1998 and have gathered 107 data points over a total time span of 1435 days.

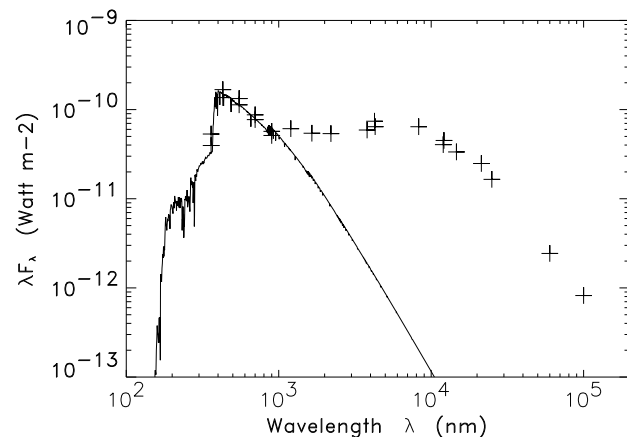


Fig. 1. The SED of IRAS 08544. For the optical measurements, the minimal and maximal fluxes are displayed. The photometric data are given in Table 2. The dereddened fluxes are shown using a total reddening of $E(B - V) = 1.45$ with the standard reddening law. Note the broad IR excess starting already at H .

2.2.4. CO measurements

CO measurements were performed with the 15 m Swedish-ESO submillimeter telescope (SEST) at La Silla. A dual channel SIS receiver was used to observe simultaneously at 115 GHz (the $J = 1-0$ line) and at 230 GHz (the $J = 2-1$ line). At 115 GHz the half power beam width and the main beam efficiency of the telescope are 45'' and 0.7 and at 230 GHz 23'' and 0.5. Typical receiver temperatures are 110 K (115 GHz) and 150 K (230 GHz). Three Acousto Optical Spectrometers (AOS) were used as backends. The 230 GHz receiver was connected to a high resolution spectrometer (HRS) and a low resolution spectrometer (LR1), the 115 GHz receiver to a second low resolution spectrometer (LR2). Five exposures were taken in the period from October 1999 to August 2001. The system temperatures for the CO ($2-1$) observations varied between 250 K and 350 K. The intensity scales, reported in Fig. 9 and Table 4, are given as main beam brightness temperature, $T_{MB} = T_A^*/\eta_{MB}$, where T_A^* is the antenna temperature corrected for atmospheric attenuation using the chopper wheel method and η_{MB} is the main beam efficiency.

Additionally we mapped the environment of IRAS08544 with low resolution spectra of ($J = 2-1$) CO on July 28th 2000. A map spacing of 11'' was used. Finally, also one low resolution ($J = 1-0$) HCN spectrum was taken. No line was detected to an r.m.s. level of 0.003 in T_{MB} . For all observations we used dual beam switching, where the source is alternately placed in the signal and the reference beam, using a beam throw of about 12'.

Table 2. The photometric data used to construct the SED. For the optical and near-IR photometry, the mean magnitude, the standard variation (σ) and the number of observations (N) is shown. The IRAS and MSX fluxes are given in Jansky. The IRAS quality label and for MSX the percent error is shown.

	<m>	σ	N	λ	flux	error
U	11.85	0.06	103	12 μm	180.30	
B	10.31	0.05	103	25 μm	158.80	
V	9.13	0.03	103	60 μm	56.25	:
R_C	8.14	0.03	103	100 μm	28.43	L
I_C	7.11	0.03	103	B1 (4.29 μm)	80.17	9.7
J	5.65	0.02	2	B2 (4.25 μm)	91.45	9.1
H	4.67	0.02	2	A (8.28 μm)	163.09	5
K	3.51	0.02	2	C (12.13 μm)	173.50	3
L	1.59	0.02	2	D (14.65 μm)	156.70	4
				E (21.34 μm)	171.57	6

3. Spectral Energy Distribution (SED)

All photometric data used in constructing the SED are given in Table 2. The optical coordinates of the Guide Star Catalogue optical object is some 19'' west, and 7'' north of the IRAS position and on the edge of the 95% positional uncertainty ellips as given in the IRAS point source catalog. The near-IR images obtained with the PICNIC camera (Glass 1999) in *J*, *H* and *K* did not show other near-IR sources which might be connected with the IRAS source. Moreover, the MSX (Egan et al. 1999) position shows a correct association with the optical source so we can safely assume the IRAS fluxes are associated with the optical component as well.

The spectral energy distribution is shown in Fig. 1. The full line represents the Kurucz model with the parameters obtained from analysis of the FEROS spectrum (see Sect.7). The total reddening of $E(B-V)=1.45$ is found by minimizing the difference between the dereddened fluxes in the optical and in the J-band and the model atmosphere. A rough estimate of the interstellar component of the reddening can be obtained using the relation between the DIB strength at 5780 and 5797 Å and the reddening (Krelowski et al. 1999). There is a rather large scatter in this relation (correlation coefficient 0.8-0.89) but we obtain a $E_{IS}(B-V)=0.7\pm 0.2$.

With $[12]-[25] = 1.42$ and $[25]-[60]=0.75$ IRAS 08544 falls clearly into the 'RV Tauri' box of the colour-colour diagram which is shown in Fig. 3(c) of Lloyd Evans (1985). Moreover, IRAS 08544 shows a very broad IR excess, which starts already at *H* (1.65 μm) and points to the presence of hot dust in the close environment of the star. Also this hot circumstellar dust component is an observed feature for RV Tauri stars (Gehrz 1972; Gehrz & Ney 1972; Lloyd Evans 1985), although compared to the RV Tauri stars studied in the last reference, the excess in *H*, *K* and *L* for IRAS 08544 is large.

This near-IR excess is generally not observed in single post-AGB stars with an expanding dust shell. It is, however, not unique and several post-AGB stars also show a similar SED with a broad-IR excess. All these latter objects turned out to be binaries and for these objects the near-IR excess is interpreted as coming from hot dust which is stored in a dusty disc. The indirect and direct evidence for this interpretation is given in Van Winckel (2001) and references therein. For several objects, the disc is resolved (e.g. AC Her, Jura et al. 2000).

We conclude that the SED of IRAS 08544 shows a very broad IR excess around a weakly variable F-type central star, which indicates the presence of a circumstellar disc instead of a freely expanding outflow. Its IR colours are very similar to those of the bulk IRAS detected RV Tauri stars.

4. Pulsations

IRAS 08544 is clearly variable, albeit with a small peak-to-peak amplitude of 0.17 mag in *V* and 0.23 mag in *B*. Since IRAS 08544 has the same IR properties as RV Tauri stars, we checked whether we for similar photospheric pulsation characteristics. The photometric data set did not enable us to recover a clear period. The long run of observations in a single season with the APT covers 131 days (see lower panel Fig. 2); the shallow 'secondary minimum', which is a defining feature of the RV Tauri stars might be present (see lower panel Fig. 2), but we lack a long enough continuous time series to label the light curve as due to a genuine RV Tauri pulsation. The pulsation time-scale seems to be typical for RV Tauri stars. The successive deep minima do not repeat well, however. The full data set has been analyzed using three period finding methods but no clear conclusions on pulsational timescales could be reached. We found two periods of nearly equal probability, 71.9 and 89.9 days. Additionally, the observations were plotted against all periods at one day intervals from 67 to 110 days as well as the double periods near 144 and 180 days and periods of 50.4 and 216 days suggested weakly by the period-finding programs, and no other plausible periods were found. The substantial scatter, with for example two exceptionally bright points (JD 2451608 and 9, see upper panel Fig. 2) somewhat remote in time from other observations, is observed also in genuine RV Tauri stars. The observational errors are not negligible compared to a *V* peak-to-peak amplitude of only 0.17 mag. The colors vary such that $B-V$ and $V-I$ are bluest when the star is bright; there is no significant phase difference and the amplitudes are only 0.02 to 0.03 mag. The $U-B$ plot is dominated by intrinsic and observational scatter.

IRAS 08544 is no genuine high amplitude RV Tauri star but is variable with a small amplitude on a similar timescale.

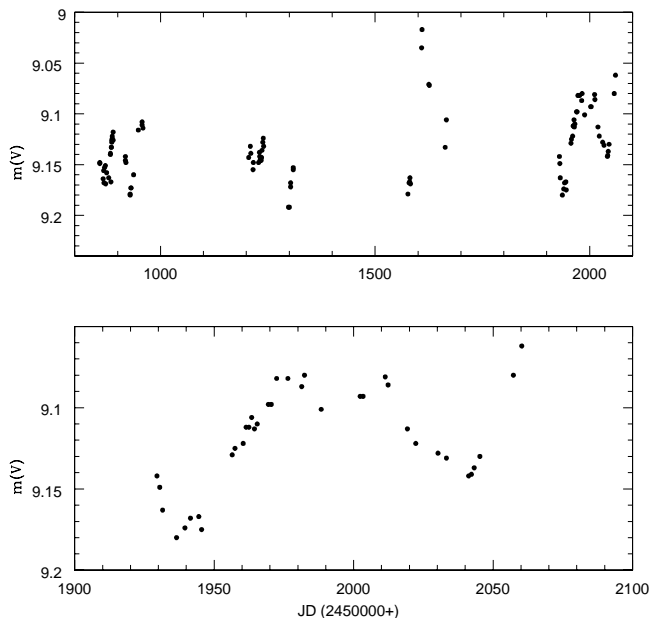


Fig. 2. The V-band photometric variations displayed by IRAS 08544 : upper panel : all photometry, lower panel : only the APT photometry. The amplitude is low (ΔV peak-to-peak = 0.17 mag) and the pulsation time-scale is near 100 days.

5. Spectral monitoring

The main purpose of our spectral monitoring is to obtain radial velocity measurements by cross-correlation of IRAS 08544, hence the signal-to-noise of every spectrum is kept low. As an interesting byproduct, we can study the variability of large features, like the $H\alpha$ -profile. In the spectra of RV Tauri stars line deformation and even line splitting is observed. They are commonly ascribed to a passage of a shock moving through the atmosphere (Gillet et al. 1989; Lèbre & Gillet 1991; Gillet et al. 1990; Fokin 1994). A cross-correlation profile is a good tracer of this motion in the photosphere (Maas et al. 2002). For IRAS 08544 deformations are sometimes present in the cross-correlation profiles (Fig. 3), but they are small, indicating that the shock is weak. The Gaussian cross-correlation profiles obtained with a proper mask for IRAS 08544 result in precise radial velocity measurements (Fig. 3) and symmetric profiles.

5.1. Radial velocities

The online reduction software for CORALIE provides cross-correlation profiles computed with a standard template of spectral type F. As we have a high signal-to-noise FEROS spectrum, we decided to use this spectrum to construct a proper template tuned for IRAS 08544 to increase the efficiency of the cross-correlation technique. The template spectrum consists of box-shaped emission lines with equal amplitudes. These lines were taken from the stan-

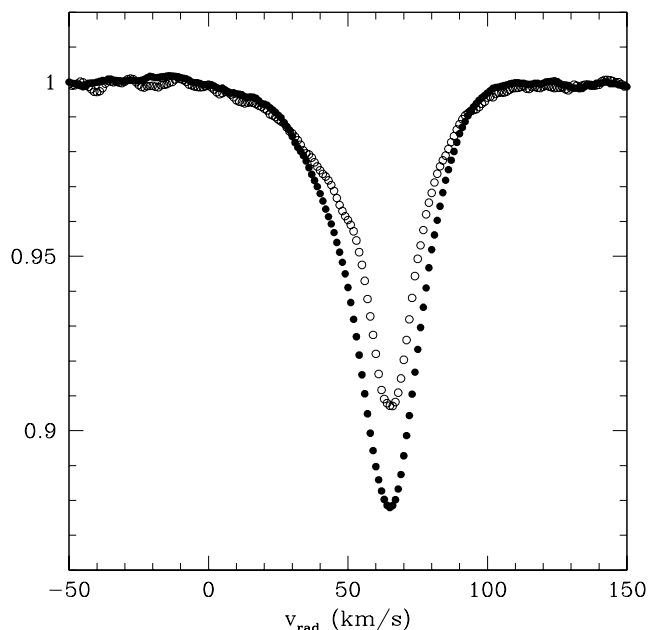


Fig. 3. Comparison between the cross-correlation profiles obtained with a standard template (open circles) and a specific template for IRAS 08544 (full circles).

standard template but only the lines, which are present in the FEROS spectrum and for which we could determine the FWHM, were selected for the IRAS 08544 template. We used this FWHM of the Gaussian fit as the width of the lines. In this way we reduced the original 3074 line mask to a mask of only 953 lines. In Fig. 3 we compare the cross-correlation profile, computed with the standard template, with the one computed with the IRAS 08544 template. Qualitatively the IRAS 08544 profiles are more symmetric and the noise in the profiles is lower, resulting in nicer profiles. For both templates we fitted the cross-correlation profiles with Gaussians. The central velocities of the IRAS 08544 template are shifted with -0.17 km s^{-1} and a standard deviation of 0.24 km s^{-1} with respect to the velocities of the standard template. For the IRAS 08544 profiles we obtained a mean FWHM of 9.31 km s^{-1} and a mean depth of 0.11, for the standard profiles a mean FWHM of 7.01 km s^{-1} and a depth of 0.08. The IRAS 08544 template results, thus, in broader and deeper profiles than the standard template.

We have accumulated 107 radial velocities, for which an orbital period of 499 days was found. Fig. 4 (upper panel) presents the radial velocities folded on the orbital period and the best least-square fit. The orbital elements are listed in Table 3. Our dataset covers 2.9 orbital cycles and the standard deviation of the O-C values for the whole data set is 1.06 km s^{-1} . For the eccentricity we obtained a value of 0.14. Applying the criterion of Lucy & Sweeney (1971), we find the eccentricity to be significant ($p=6.9 \cdot 10^{-3} \%$). Assuming an average inclination of 60° and a mass of $0.6 M_\odot$ for IRAS 08544, we find for the unseen companion a mass of $0.3 M_\odot$. The companion could be

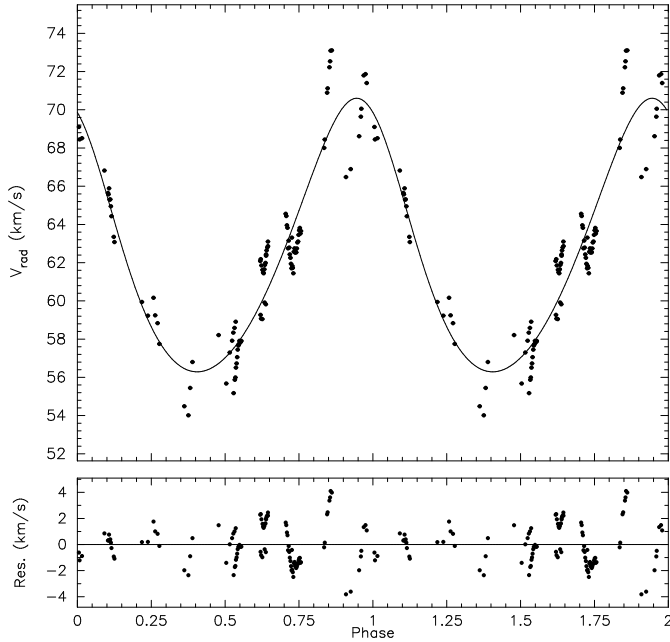


Fig. 4. Upper panel : The heliocentric radial velocity data folded on the 499 day period. The full line is the radial velocity fit discussed in the text. Phase 0 corresponds to periastron passage. Lower panel : the residuals for the radial velocities for the 499 day period fit.

Table 3. The orbital elements of IRAS 08544.

	IRAS 08544	
		σ
Period (days)	499	3
$a \sin i$ (AU)	0.32	
F(M) (M_{\odot})	0.02	
K (km s^{-1})	7.2	0.2
e	0.14	0.02
ω ($^{\circ}$)	26	10
T_0 (periastron) (JD245+)	1964	14
γ (km s^{-1})	62.5	0.1
σ_{O-C}	1.06	
N	107	

a late-type main sequence star or a low-mass (helium) WD. A compact companion makes the evolutionary status of this object (with the non-zero eccentricity) even more puzzling.

We have analyzed the residuals (Fig. 4 : lower panel and Fig. 6) for periodicities. The θ -statistics of the PDM-method (Stellingwerf 1978) are shown in Fig. 5. We suspect variability at a timescale of 100 and/or 30 days, but we cannot prove yet that this period is stable on a longer time scale. We interpret this variability as due to pulsations.

Fig. 5. The θ -statistics of the PDM-analysis for the residuals of the radial velocities for a period of 499 days (see text). 5 bins and 4 covers were used in this analysis.

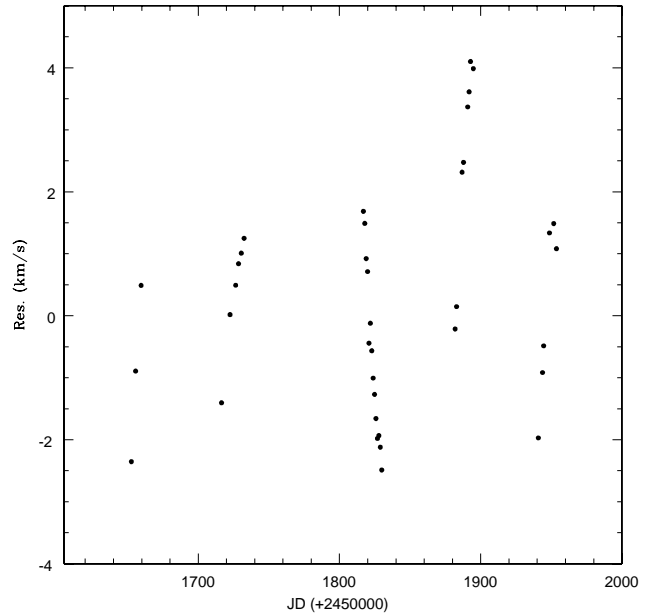
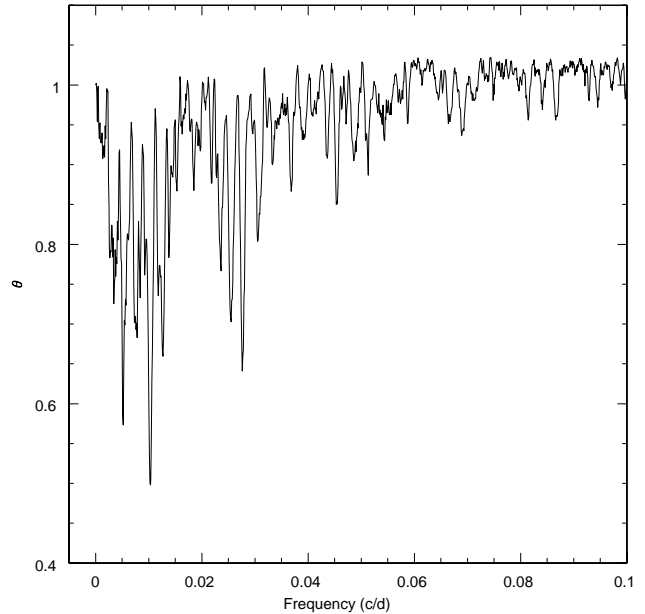


Fig. 6. The residuals from JD 2451605 to 2452000, showing a clear structure on a timescale shorter than the orbital period. The time-scale of this low amplitude scatter is around 90 days which we interpret as due to the pulsational amplitude in the radial velocity data.

5.2. $H\alpha$ -profile

In all our CORALIE spectra $H\alpha$ shows a strong P-Cygni profile of a fast stellar wind, which is highly unusual for an F-type object. The P-Cygni profile varies with time

(see Fig. 7) and indicates that the mass outflow is variable or non-spherically symmetric. As a detailed model of the outflow is needed to derive accurately parameters such as the expansion velocity and the mass loss rate, we will only determine the order of the expansion velocity and describe the observational characteristics of the profile. We took as the expansion velocity, the velocity of the intersection of the continuum level and the tangent in the bending point in the absorption component of the P-Cygni profile, and found that it varies between 100 and 400 km s⁻¹! The EW of the absorption component (integrated between the wavelength of the expansion velocity and that of the intersection of the H α -line and the continuum level) varies between 1 and 5 Å. Fig. 8 shows that both the expansion velocity and the EW of the absorption component of H α are correlated with the orbital phase and reach a maximum between phase 0.13 and 0.26. This is around superior conjunction at phase 0.16 : i.e. when the primary is at its farthest position with respect to us and the secondary at its nearest. Thus assuming the F-type star is the H α emitter in the binary system, the mass outflow is not spherically symmetric but seems to reach a maximum in the direction of the companion. The intensity of the emission peak varies from 1.3 to 1.8 times the continuum level. As the H α -emission intensity is very sensitive to the mass loss rate (Kunasz & Morrison 1982), the mass loss rate of IRAS 08544 seems to be variable during orbital motion. Finally, the variation of the EW of the emission component is smaller than that of the absorption component and lies in the range of 0-2 Å. In some spectra an extra small blue shifted emission or a slight recovery between two absorption components is observed (see upper spectrum in Fig. 7). Just before publication two additional observations were inserted. They correspond to orbital phases 0.22 and 0.24 and do not show the high expansion velocity and high absorption EW expected from the preceding cycles. However, their expansion velocity is still higher than those between phases 0.35 and 1.0. This could indicate that there is a orbital cycle to cycle variation in the strength and velocity of the H α -absorption.

For the moment neither the origin nor the location in the system of the fast H α -emitting gas is understood.

6. CO mm-wave line emission

6.1. CO ($J=1-0$) and ($J=2-1$) emission lines

The CO data for IRAS08544 are shown in Fig. 9. For all spectra a baseline is subtracted. The random mean scatter in the spectra outside the line is of the order of 0.02 K. In Table 4 the central heliocentric velocities, the FWHM and the integrated intensities, obtained by Gaussian fitting, for the different lines are presented.

The central velocity of the low resolution CO (2-1) line taken on 2/10/99 (Fig. 9, upper panel), which corresponds to an orbital phase of 0.94, is 61.3 km s⁻¹. However, our CORALIE data (see Fig. 4) point to a photospheric velocity of 70.6 km s⁻¹ at this orbital phase. The variation

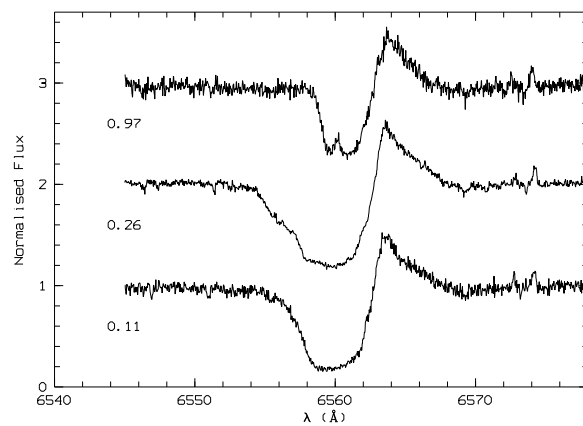


Fig. 7. The variable P-Cygni profile of H α . The orbital phase is indicated for each spectrum.

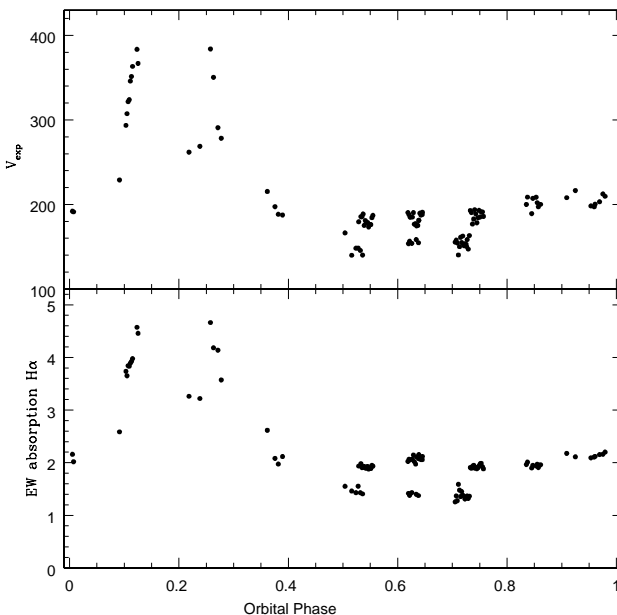


Fig. 8. The expansion velocity (upper panel) and the EW of the absorption component of the P-Cygni profile of H α (lower panel) versus the orbital phase.

Table 4. The central heliocentric velocity (km s⁻¹), the FWHM (km s⁻¹) and the integrated intensity (K km s⁻¹), obtained by Gaussian fitting, for the different lines. The second quoted line is the central position of the map shown in Fig. 10.

line	V_c	FWHM	I_{CO}
CO (2-1) LRS 2/10/99	61.3	6.3	2.8
CO (2-1) LRS 28/07/00	61.3	6.4	3.1
CO (2-1) HRS total	60.7	5.9	2.3
CO (1-0) LRS total	61.7	5.4	0.9

due to pulsation can not explain the difference between the orbital velocity and the velocity derived from the CO

line. This means that the CO emission is not following the orbital motion of IRAS08544.

Comparing the two low resolution spectra of the CO (2-1) line, observed at 2/10/99 and 28/07/00 (Fig. 9, first and second panel respectively), the latter being the spectrum of the central position of our map, we state that both have the same central velocities. This is valid for all our profiles. We can thus conclude that the central velocity of the CO lines is constant. It traces the motion of the system and not that of the primary star. However, a small difference is found between the central velocity (60.7 km s^{-1} , taken from the averaged HRS CO (2-1) line) and the system velocity of 62.5 km s^{-1} derived from the CORALIE data.

The CO emission of IRAS08544 is weak compared to its $60 \mu\text{m}$ flux. For AGB-stars a correlation is observed between the integrated intensity of the CO (1-0) line and the $60 \mu\text{m}$ flux (Nyman et al. 1992). Also single post-AGB stars like the 21 μm objects follow this correlation (Van Winckel et al. 1999). Using this correlation for oxygen rich stars, the observed $60 \mu\text{m}$ flux of 56 Jansky for IRAS08544 corresponds to an integrated intensity of the CO (1-0) line of 5.5 K km s^{-1} . This is a factor 6 higher than the observed CO (1-0) integrated intensity ($I_{CO} = 0.92 \text{ K km s}^{-1}$). With respect to the $60 \mu\text{m}$ flux coming from the dust, the circumstellar environment of IRAS08544 is deficient in CO, which is common in RV Tauri objects (Alcolea & Bujarrabal 1991; Van Winckel et al. 1999).

The triangular line shape of the CO lines is peculiar and differs from the CO line shape expected for a mass-losing (Post)-AGB star. For a spatially unresolved mass-losing (Post)-AGB star the CO line is rectangular for a low optical depth and parabolic for a high optical depth (Olofsson et al. 1993). For 89 Her, AC Her, HD 44179 (the central star of the Red Rectangle), BM Gem and EU And a similar line profile as for IRAS08544 is observed (Likkell et al. 1991; Alcolea & Bujarrabal 1991; Bujarrabal et al. 1988; Jura et al. 1995; Jura & Kahane 1999). All these objects show a weak and small CO emission component with a FWHM in the range of $0.5\text{-}5 \text{ km s}^{-1}$ and for the latter four Jura & Kahane (1999) argue that these emission components are the signatures of long-lived reservoirs of gravitationally bound gas. With a FWHM of 6 km s^{-1} , IRAS08544 falls slightly out of this range, but a higher inclination angle of the orbital plane can increase the FWHM of the CO emission line.

We conclude that the CO line-profile of IRAS08544 is also indicative for the presence of gravitationally bound gas in a circumbinary disc. Note that due to the misclassification of the LRS IRAS spectrum, this object was observed and detected also in the CO survey of infrared carbon stars by Groenewegen et al. (2002). We checked the profile of Groenewegen et al. (2002), the velocity is the same but they used the half-width-zero-intensity to compute the outflow velocity for which they derive 8.2 km s^{-1} . We checked their line-profile which was kindly given to us

but since we obtained a high S/N high-resolution spectrum, we used our detection in what follows.

To obtain a rough lower bound for the mass contained in the CO envelope we follow the train of thought of Jura & Kahane (1999), Jura et al. (1997) and Kahane et al. (1998). As an approximation we assume that the gas is in circular orbits around the binary system for which we adopt a mass of $0.9 M_{\odot}$ ($0.6 M_{\odot}$ for the Post-AGB star + $0.3 M_{\odot}$ for the companion). We estimate the inner radius, R_{in} of the disc from the CO line FWHM. If V_{orb} denotes the orbital velocity of the gas,

$$R_{in} = GM/V_{orb}^2 \quad (1)$$

With $V_{orb} = 3 \text{ km s}^{-1}$ from our CO (2-1) high resolution line, $R_{in} = 90 \text{ AU}$. The luminosity of IRAS08544 lies in the range of $3000\text{-}7000 L_{\odot}$. We adopt here a value of $5000 L_{\odot}$. At a distance of 90 AU from the star with a luminosity of $5000 L_{\odot}$ a blackbody grain has a predicted temperature of 250 K .

If the gas is optically thin we can crudely estimate the column density of CO molecules in the beam, $\overline{N(CO)}$

$$\overline{N(CO)} = \frac{3k^2 T_{ex}}{4\pi^3 \mu^2 h \nu^2} \int T_{mb} dv \quad (2)$$

where μ is the dipole moment of the CO molecule (0.1098 D ; Chackerian & Tipping 1983) and ν is the frequency of the (2-1) transition (230.538 GHz). In this equation several assumptions have been made: (1) the microwave background is ignored, (2) the partition function scales as kT_{ex} and (3) the Planck function and the correction term for stimulated emission can be simplified by linear expansion of $\exp(\pm h\nu/kT_{ex})$. We find $\overline{N(CO)} \simeq 6 \times 10^{15} \text{ cm}^{-2}$.

The total mass of CO molecules (M_{CO}) in the beam is the product of $\overline{N(CO)}$, the mass of a CO molecule (m_{CO}) and the projected area of the beam on the sky A_{beam} . For a beam assumed to be Gaussian with half-power diameter θ_{HPBW} ,

$$A_{beam} = \pi \theta_{HPBW}^2 D_*^2 / (4 \ln 2) \quad (3)$$

with D_* the distance to the star. If we adopt a distance of 1 kpc , we find $M_{CO} = 3.6 \times 10^{25} \text{ kg}$. With the assumption of $[CO/H] = 10^{-4}$, the total mass in the CO envelope is $0.2 M_{\odot}$. If the gas is optically thick, this value is a lower bound.

6.2. CO map

We mapped the environment of IRAS08544 in low resolution CO(2-1). The CO map consists of 14 positions with a spacing of $11''$ and is presented in Fig. 10. The clear maximum observed in the central position of the map, which is also presented in the second panel of Fig. 9, indicates that the CO line is not interstellar. We find that an asymmetry is present in the map: while positions (-1,1) and (1,-1) show a clear CO emission, the intensity of the CO emission is lower in position (1,1) and CO emission is absent in position (-1,-1). This could mean that the CO emission

is anisotropic and extended. However, this asymmetry can also be caused by pointing errors in the different positions of the map, which can also explain the signal present in the position (2,0).

7. Chemical composition

7.1. Atmospheric Parameters

The abundances are calculated on the basis of a LTE model atmospheres of Kurucz (1993) and the LTE program MOOG of Sneden. A model atmosphere is determined by its effective temperature (T_{eff}), the gravity ($\log g$) and the metallicity ($[Fe/H]$). We determined these parameters on the basis of spectroscopic criteria : the effective temperature by forcing the abundances of Fe I-lines to be independent of the excitation potentials and the gravity by forcing ionization balance between the Fe I and Fe II lines. Moreover, the microturbulent velocity was estimated by forcing the abundance of the FeI-lines to be independent of the reduced equivalent width. We then used the model atmospheres with the correct overall metallicity as given by the Fe abundance. The oscillator strengths of the lines were taken from the critically compiled database continuously updated in our institute. For more details we refer to Van Winckel & Reyniers (2000).

We obtained $T_{eff} = 7250$ K, $\log g = 1.5$ and $[Fe/H] = -0.5$ for the model parameters. This temperature is in agreement with the spectral type F3 determined from low resolution spectra and confirms the position of IRAS 08544 on the high temperature side of the instability strip.

7.2. Results

The abundance results obtained for IRAS 08544 are listed in Table 5. In Fig. 11 the abundance of the elements are plotted versus their dust condensation temperature. The spectrum has a high S/N of 150 (measured around 5800 Å) and we used a total of 264 lines, restricting ourselves to small lines ($EW \leq 150$ mÅ). These lines have, like all the other lines in the spectrum, symmetric profiles (see Fig. 12 and 13). The good consistency between the abundances derived from the different ionization levels for the elements Cr, Mn, Ni confirms the reliable model atmosphere parameters.

With $[Fe/H] = -0.3$ and $[Zn/Fe] = +0.4$ IRAS 08544 displays a weak signature for depletion of refractory elements in its photosphere. In Fig. 11 we can distinguish two groups of elements. For elements like C, N, S, Zn, Na, Ba, Cu there is no correlation between the abundance and the condensation temperature. For elements with a condensation temperature higher than about 1200 K the abundance goes down from -0.2 for $[Cr, Mn, Ni/H]$ to -1.1 for $[Zr/H]$, as the condensation temperature increases. One element doesn't really fit in this picture which is Si. Lodders & Fegley (1988) give a condensation temperature of 1529 K for Si. However in the notes they say that most Si condenses into $MgSiO_3$ and Mg_2SiO_4 which has a con-

Table 5. Chemical analysis of IRAS 08544 . For the solar iron abundance we used the iron meteoric abundance of 7.51. For the solar C,N and O abundances we adopted resp. 8.57, 7.99 and 8.86 (C: Biémont et al. 1993, N: Hibbert et al. 1991, O: Biémont et al. 1991). For the solar Mg and Si abundances we adopt 7.54 (Holweger 2001); the other solar abundances are taken from Grevesse & Sauval (1998). The dust condensation temperatures are from Lodders & Fegley (1988) and references therein. They are computed using a solar abundance mix at a pressure of 10^{-4} atm. They do not ascribe a condensation temperature to O as it is the most abundant element in rock and therefore a separate condensation temperature is meaningless. For all ions, the number of lines, the mean equivalent width, the absolute abundance and the σ of the line-to-line scatter are given.

IRAS 08544						
$T_{eff} = 7250$ K						
$\log g = 1.5$						
$\xi_t = 4.50$ km s $^{-1}$						
$[Fe/H] = -0.5$						
ion	N	\overline{W}_λ	ϵ	σ	[el/H]	T_{cond}
C I	21	68	8.55	0.13	-0.02	78
N I	3	81	8.19	0.15	0.20	120
O I	4	49	8.67	0.05	-0.19	
Na I	6	42	6.48	0.05	0.15	970
Si I	9	26	7.60	0.11	0.06	1529
S I	6	56	7.45	0.07	0.12	674
Ca I	13	69	6.00	0.11	-0.36	1634
Sc II	5	85	2.30	0.10	-0.87	1652
Ti II	16	75	4.17	0.10	-0.85	1600
Cr I	11	34	5.46	0.15	-0.21	1301
Cr II	16	91	5.46	0.13	-0.21	
Mn I	5	50	5.22	0.12	-0.17	1190
Mn II	1	41	5.20		-0.19	1190
Fe I	83	55	7.19	0.13	-0.32	1337
Fe II	39	66	7.16	0.15	-0.35	
Ni I	16	29	6.03	0.12	-0.22	1354
Ni II	1	27	6.00		-0.25	1354
Cu I	1	19	4.30		0.09	1170
Zn I	2	81	4.69	0.03	0.09	684
Y II	3	16	1.30	0.18	-0.94	1622
Zr II	1	6	1.52		-1.08	1717
Ba II	1	131	2.27		0.14	1162
La II	1	13	0.48		-0.69	1520
Nd II				< 0.84	< -0.66	1563

densation temperature of 1340 K. This lower temperature would improve the position of Si in our interpretation of Fig. 11.

To verify the depletion pattern observed in Fig. 11, we also calculated the abundances on the basis of two other model atmospheres. The first model has the parameters $T_{eff} = 7500$ K, $\log g = 2.0$ and $[Fe/H] = -0.5$, the second the parameters $T_{eff} = 7000$ K, $\log g = 1.5$

and $[\text{Fe}/\text{H}] = -0.5$. For the first model there is a global upward shift with a mean of 0.16, for the second model a global downward shift with a mean of 0.13. However, the typical depletion pattern is conserved for both models. Moreover, the abundance ratios $[\text{S}/\alpha]$ ($\alpha = \text{Si}, \text{Ca}$ and Ti) and $[\text{Zn}/\text{Fe}]$ which trace the depletion of a photosphere, are almost independent of the model used. For the first model we obtained $[\text{S}/\alpha]=0.45$ and $[\text{Zn}/\text{Fe}]=0.42$, for the second $[\text{S}/\alpha]=0.54$ and $[\text{Zn}/\text{Fe}]=0.35$ (compared to $[\text{S}/\alpha]=0.50$ and $[\text{Zn}/\text{Fe}]=0.43$ for our preferred model). So we can conclude that the depletion is small but real.

The small N-overabundance ($[\text{N}/\text{H}]=+0.2$) might be the consequence of a first dredge-up. As the C-abundance is solar and the s-process elements follow the depletion pattern, there is no evidence for dredge-up of material processed by nucleosynthesis on the AGB.

For the s-process element Nd we could only derive an upper limit since even the strongest expected lines were not present in the spectra. The upper limit is therefore derived assuming a fixed EW of 5 mÅ for the strongest line in a clear part of the spectrum. We used the line lists of the Vienna Atomic Line Database (Vald2, <http://www.astro.univie.ac.at/vald/>, Kupka et al. 1999) to look for these strongest optical lines.

We also noted a P-Cygni profile for two FeI lines, at 5576.089 Å and at 6400.001 Å. We also detected 9 emission lines in the spectrum (7 of FeI, 1 of CaI and 1 of TiI). All these lines have low excitation potentials.

To summarize, IRAS08544 is a star where the depletion process has slightly altered the photospheric abundances ($[\text{Zn}/\text{Fe}] = +0.4$) and for which there is no evidence for typical 3rd dredge-up chemical enrichment.

8. Conclusions and discussion

The main conclusions obtained from the analysis of our large data-set are :

- 1) IRAS08544 is not a carbon star as listed in the literature but an F-type post-AGB star with IR colours similar to the bulk of the IRAS detected RV Tauri stars;
- 2) The star shows variability with a small amplitude ($\Delta V=0.17$) for which the time-scale (between 30-100 days) is not repeating well;
- 2) IRAS 08544 is a binary system with a period of 499 ± 3 days and a significant non-zero eccentricity of 0.14 ± 0.02 ;
- 3) the SED shows a broad IR-excess, indicating beside the presence of cold circumstellar dust also the presence of a strong hot dust component indicative of a circumbinary disc;
- 4) the weak CO emission line and its triangular shape also points to a circumbinary location with a low gas-to-dust ratio;
- 5) The $\text{H}\alpha$ -line shows a P-Cygni profile for which both the strength and outflow velocity are correlated with the orbital period with maxima at superior conjunction;
- 6) the photosphere is moderately depleted in refractory

elements ($[\text{Zn}/\text{Fe}]=+0.4$).

IRAS08544 was selected on the basis of its IRAS colours which fall into the RV Tauri box as defined by Lloyd Evans (1985). Kwok et al. (1997) classified IRAS sources on the basis of their IRAS low-resolution spectra. They report the detection of circumstellar $11 \mu\text{m}$ SiC dust emission for IRAS08544 and classify the star as a possible carbon star. Our optical data clearly identifies the star as an F-type object and also the oxygen rich nature of the photosphere derived in our chemical abundance analysis does not agree with a post-carbon star spectrum. Examination of the LRS spectrum (Olson et al. 1986) shows that the $18 \mu\text{m}$ silicate band is present in the form of weak emission, while the structure near $10 \mu\text{m}$ may be understood as the $9.7 \mu\text{m}$ silicate band with central reversal and low contrast. The spectrum therefore shows self-absorption. An alternative classification on the original scheme of Olson et al. (1986) would be 31, indicating silicate absorption. Silicate self-absorption is explicitly taken into account in the system of Lloyd Evans (1990), where the appropriate classification would be 21BA. The equivalent on the new KSPW system (Kraemer et al. 2002) is 3.SB or 4.SB. This reclassification removes the anomaly.

Lloyd Evans (1999) determined an RV Tauri instability strip based on the RV Tauri stars listed in the GCVS. The amplitude of IRAS 08544 is small for an RV Tauri star and its spectral type places it outside and on the hot side of this instability strip. This suggest that the star has almost left the classical instability strip towards the phase of the planetary nebulae. Despite its probably more evolved nature, the infrared colours of IRAS 08544 are very similar to the IRAS detected RV Tauri stars.

Moreover, IRAS08544 is a binary with a period of 499 days together with a significant eccentricity of 0.14 which is difficult to explain in terms of a previous standard binary AGB-evolution. On the AGB, the orbit was too small to accommodate an M-star with the same luminosity and it is not clear how the star avoided spiral-in, leading to a circular orbit of short period. Post-AGB binaries are not uncommon and other objects with similar orbits and large eccentricities were observed (e.g. Waters et al. 1997; Van Winckel 2003). Population synthesis codes have shown that systems of post-AGB stars with resulting periods in the order of one hundred to a few hundred days can only be expected if an efficient tidally enhanced mass-loss is induced. This wind increases the mass-loss significantly prior to Roche-lobe overflow (RLOF) and decreases the envelope binding energy to avoid spiral-in to very short orbits. Following Pols et al. (2003) no eccentric systems with $P < 3000$ days are produced; this is at variance with earlier reports by Karakas et al. (2000). IRAS 08544 is another binary with a rather short period and eccentric orbit in an apparent post-AGB evolutionary phase for which the mere existence is not very well understood in binary stellar evolution theory.

It has been known for some time that a subset of those post-AGB binaries are extremely depleted (e.g.

Van Winckel et al. 1995). The depletion process implies that the star is coated with a gaslayer, from which the dustgrains were removed, probably by radiation pressure. Since dust formation is thought to occur in the circumstellar environment and not in the photosphere, the process involves re-accretion of circumstellar gas. Mathis & Lamers (1992) have discussed several processes in which separation of circumstellar dust and gas may operate and Waters et al. (1992) added that the most favorable circumstances may occur if the circumstellar dust is trapped in a stable disc. For post-AGB stars the presence of a circum-system disc implies binarity and the observational basis of this process was that all strongly depleted objects known at that time were found to be binaries with strong evidence for some of them that the dust was indeed in a flattened geometry (Van Winckel et al. 1995).

The binary prerequisite for the depletion process was disputed, however, after the recent finding that many RV Tauri stars are also depleted. Preston et al. (1963) subdivided the RV Tauri stars into three spectroscopic classes (RVA,RVB,RVC) : RVA have spectral type G and K and show strong metallic lines and have normal CN and CH bands. RVB have spectral type Fp(R), they are weak-lined but show enhanced CN and CH bands. RVC are also weak lined objects with spectral type Fp but with normal CN and CH bands. There is now general agreement that the abundance anomalies are mainly due to a depletion process and are not reflecting internal dredge-up processes (Giridhar et al. 1994, 1998, 2000; Gonzalez et al. 1997a,b; Van Winckel et al. 1998; Maas et al. 2002). The strength of the abundance anomalies differs from star to star. However, all the stars of the RVB class are affected, while the RVA class contains stars which are less or not affected at all. The RVC stars, which have a low initial metallicity $[Fe/H] \leq -1.0$, do not show any sign of depletion (Giridhar et al. 2000). In IRAS 08544, the depletion altered the photospheric chemical composition but only mildly so. This is well established by the significant ratios $[Zn/Fe]=+0.4$, $[S/\alpha]=+0.5$. As we have evidence for a current outflow, no accretion of gas is going on. The fractionation process has thus occurred in the past. However, the atmosphere is only slightly changed in its composition and since IRAS 08544 shows a large and broad excess, this illustrates again that no correlation exists between the strength of the *current* IR-excess and the severity of the depletion (Giridhar et al. 2000). An explanation put forward for the moderate depletion of the RVA RV Tauri stars is convection (Gonzalez et al. 1997a) : a depletion process has occurred but mixing with deeper layers with normal abundances, has diminished the effects. Convection could as well have diluted the anomalies caused by the depletion process in IRAS 08544, when IRAS 08544 was cooler and had a deeper convective envelope.

Van Winckel et al. (1999) argued that many IRAS selected RV Tauri stars are suspected binary systems where the circumstellar material resides in a stable dusty disc. Such a disc was resolved in a prototypical RV Tauri star AC Her (Jura et al. 2000) which was found to be a

binary with a period of 1200 days (Van Winckel et al. 1998). Recently, radial velocity monitoring showed that two strongly depleted RV Tauri stars, RU Cen and SX Cen, are indeed members of binary systems (Maas et al. 2002). Moreover, the orbital period of SX Cen is around 600 days, which is similar to the period of the long term photometric variation in the light curve. This indicates that the long term photometric variation in SX Cen is due to variable circumstellar reddening and that the photometric class of the RV Tauri stars has its origin in a difference in inclination angle : the RVb RV Tauri stars are seen near edge on and the variable circumstellar reddening is due to the circumbinary disc, which is in the line of sight. The RVA RV Tauri stars are seen face on and no long term photometric variation is present (Van Winckel et al. 1999). The binary system IRAS 08544 clearly fits in this picture. The hot dust observed in IRAS 08544 was not ejected recently but in a previous phase in which it was stored close to the star.

Another interesting analogue to IRAS 08544 is 89 Her. It is a semiregular variable (pulsation period = 62 days, Fernie 1981) of spectral type F2. It is a binary system with an orbital period of 288 days and an eccentricity of 0.19 (Waters et al. 1993). The SED shows a broad IR-excess and the CO emission profile has a very narrow central peak with a width of less than 1 km s^{-1} (Likkell et al. 1991; Alcolea & Bujarrabal 1991). Interferometric CO observations of 89 Her reveal the presence of two distinct shells (Alcolea & Bujarrabal 1995). The outer shell lies at a distance of about $5 \times 10^{16} \text{ cm}$ from the star and corresponds to the mass ejection in the AGB-phase, which stopped more than 1000 years ago (using an expansion velocity of 7 km s^{-1}). The inner shell has an outer radius of 10^{16} cm . The $H\alpha$ -line shows also a P-Cygni profile with an outflow velocity of 150 km s^{-1} (Sargent & Osmer 1969). The chemical analysis of the photosphere performed by Luck et al. (1990) proves, however, that no depletion process has taken place in 89 Her. Waters et al. (1993) proposed for 89 Her a model in which dust has been stored in a circumbinary disc while no dust is formed in the low density outflow. In the plane of the disc the ejected material is decelerated. In the polar regions there is a free outflow. A similar model could be applicable to IRAS 08544. However, our $H\alpha$ monitoring indicates that the maximal outflow velocity is towards the companion, not the poles (in which case a constant outflow velocity would be observed). Emission lines are observed in the spectrum of 89 Her, as they are in IRAS 08544. These emission lines could be collisionally excited as the wind of the central star runs into the circumsystem disc (Waters et al. 1993).

On the basis of the triangular shape and the weakness of the CO line IRAS 08544 is similar to other similar objects : AC Her, HD 44179 (the central star of the Red Rectangle), BM Gem and EU And. In these objects (a part of) the CO emission is coming from an orbiting molecular reservoir (Jura & Kahane 1999). The objects BM Gem and HD 44179 show, beside a small emission component, also a broad weaker component, probably coming from a

bipolar outflow. As the CO disk component is extremely small, the two components are clearly distinguishable. It is tentatively suggested that the CO profile of IRAS 08544 also consists of two components which are difficult to distinguish. For IRAS 08544 the CO disc component is wider and is more difficult to separate from a possible wide component.

Beside a weak and small CO emission component, there are also other observations for HD 44179 and the RV Tauri star AC Her which indicate that the physical and chemical conditions in a circumbinary disc are different from those observed in an outflow : ISO-SWS spectra reveal a high abundance of oxygen-rich crystalline silicates (Waters et al. 1998; Molster et al. 1999) and a very strong millimeter continuum flux from large dust grains is present (van der Veen et al. 1994; Shenton et al. 1995). IR spectra are needed to verify whether these features are also present in IRAS 08544 . The photospheres of these three objects are depleted, but with variable strength : $[\text{Fe}/\text{H}] = -0.3$ and $[\text{Zn}/\text{Fe}] = +0.4$ for IRAS 08544 , $[\text{Fe}/\text{H}] = -1.7$ and $[\text{Zn}/\text{Fe}] = +0.7$ for AC Her (Van Winckel et al. 1998) and $[\text{Fe}/\text{H}] = -3.3$ and $[\text{Zn}/\text{Fe}] = +2.7$ for HD 44179 (Waelkens et al. 1996). The conditions under which the depletion process (whether or not covered by mixing) is highly efficient, of average efficiency or not at all efficient, is still not clear and needs further investigation.

We conclude that IRAS 08544 is an interesting post-AGB binary with many characteristics of RV Tauri stars and which evolved probably just outside the instability strip. More detailed study, especially at high angular resolution of IRAS 08544 and other similar objects will help us to clarify the relation between the characteristics and evolution of the circumstellar environment, the binary nature of the object and the presence of the depletion process. Moreover, the evolutionary link between the different post-AGB binaries needs further investigation.

Acknowledgements. We are indebted to Greg Roberts for some of the *UBVRI* photometry with the 0.5 m telescope and the Geneva Observatory for the generous awarding of telescope time on the Euler telescope as well as for the reduction and cross-correlation software. We thank Laurent Eyer, Katrien Kolenberg, Bart Vandebussche, Maarten Reyniers, Katrien Uytterhoeven, Tinne Reyniers, Roeland Van Malderen, Caroline Van Kerckhoven, Wim De Meester, Gert Raskin, Stephanie De Ruyter and Pierre Royer of the (former) staff of the Instituut voor Sterrenkunde of the KU Leuven for the monitoring observations on the Euler telescope. We thank the referee (A.A. Zijlstra) for the detailed and constructive remarks. TM acknowledges financial support from the Fund for Scientific Research of Flanders (FWO) under the grant G.0178.02.. HVW acknowledges financial support from the FWO as post-doc. The Swedish-ESO Submillimetre Telescope, SEST, is operated jointly by ESO and the Swedish National Facility for Radio Astronomy, Onsala Space Observatory at Chalmers University of Technology.

References

Alcolea, J. & Bujarrabal, V. 1991, *A&A*, 245, 499

- . 1995, *A&A*, 303, L21+
- Biéumont, E., Hibbert, A., Godefroid, M., & Vaeck, N. 1993, *ApJ*, 412, 431
- Biéumont, E., Hibbert, A., Godefroid, M., Vaeck, N., & Fawcett, B. C. 1991, *ApJ*, 375, 818
- Bujarrabal, V., Bachiller, R., Alcolea, J., & Martin-Pintado, J. 1988, *A&A*, 206, L17
- Carter, B. S. 1990, *MNRAS*, 242, 1
- Chackerian, C. & Tipping, R. H. 1983, *J. Mol. Spectrosc.*, 99, 431
- Egan, M. P., Price, S. D., Moshir, M. M., Cohen, M., & Tedesco, E. 1999, Technical Report, AD-A381933; AFRL-VS-TR-1999-1522, 14854
- Fernie, J. D. 1981, *ApJ*, 243, 576
- Fokin, A. B. 1994, *A&A*, 292, 133
- Gehrz, R. D. 1972, *ApJ*, 178, 715
- Gehrz, R. D. & Ney, E. P. 1972, *PASP*, 84, 768
- Gillet, D., Burki, G., & Duquennoy, A. 1990, *A&A*, 237, 159
- Gillet, D., Duquennoy, A., Bouchet, P., & Gouiffes, C. 1989, *A&A*, 215, 316
- Giridhar, S., Lambert, D. L., & Gonzalez, G. 1998, *ApJ*, 509, 366
- . 2000, *ApJ*, 531, 521
- Giridhar, S., Rao, N. K., & Lambert, D. L. 1994, *ApJ*, 437, 476
- Glass, I. S. 1999, *Monthly Notes of the Astron. Soc. Southern Africa*, Vol. 58, p. 147, 58, 147
- Gonzalez, G., Lambert, D. L., & Giridhar, S. 1997a, *ApJ*, 481, 452
- . 1997b, *ApJ*, 479, 427
- Grevesse, N. & Sauval, A. J. 1998, *Space Science Reviews*, 85, 161
- Groenewegen, M. A. T., Sevenster, M., Spoon, H. W. W., & Pérez, I. 2002, *A&A*, 390, 501
- Hibbert, A., Biéumont, E., Godefroid, M., & Vaeck, N. 1991, *A&AS*, 88, 505
- Holweger, H. 2001, in *AIP Conf. Proc. 598: Joint SOHO/ACE workshop "Solar and Galactic Composition"*, ed. R. F. Wimmer-Schweingruber, 23–+
- Jura, M., Balm, S. P., & Kahane, C. 1995, *ApJ*, 453, 721
- Jura, M., Chen, C., & Werner, M. W. 2000, *ApJ*, 541, 264
- Jura, M. & Kahane, C. 1999, *ApJ*, 521, 302
- Jura, M., Kahane, C., Fischer, D., & Grady, C. 1997, *ApJ*, 485, 341
- Kahane, C., Barnbaum, C., Uchida, K., Balm, S. P., & Jura, M. 1998, *ApJ*, 500, 466
- Karakas, A. I., Tout, C. A., & Lattanzio, J. C. 2000, *MNRAS*, 316, 689
- Kraemer, K. E., Sloan, G. C., Price, S. D., & Walker, H. J. 2002, *ApJS*, 140, 389
- Krełowski, J., Ehrenfreund, P., Foing, B. H., et al. 1999, *A&A*, 347, 235
- Kunasz, P. B. & Morrison, N. D. 1982, *ApJ*, 263, 226
- Kupka, F., Piskunov, N., Ryabchikova, T. A., Stempels, H. C., & Weiss, W. W. 1999, *A&AS*, 138, 119

- Kurucz, R. 1993, ATLAS9 Stellar Atmosphere Programs and 2 km/s grid. Kurucz CD-ROM No. 13. Cambridge, Mass.: Smithsonian Astrophysical Observatory, 1993., 13
- Kwok, S., Volk, K., & Bidelman, W. P. 1997, *ApJS*, 112, 557
- Lèbre, A. & Gillet, D. 1991, *A&A*, 246, 490
- Likkell, L., Forveille, T., Omont, A., & Morris, M. 1991, *A&A*, 246, 153
- Lloyd Evans, T. 1985, *MNRAS*, 217, 493
- . 1990, *MNRAS*, 243, 336
- . 1997, *Ap&SS*, 251, 239
- Lloyd Evans, T. 1999, in *IAU Symp. 191: Asymptotic Giant Branch Stars*, ed. T. Le Bertre, A. Lèbre, & C. Waelkens, Vol. 191, 453–+
- Lodders, K. & Fegley, B. 1988, *The Planetary Scientist's Companion* (Oxford University Press), 83
- Luck, R. E., Bond, H. E., & Lambert, D. L. 1990, *ApJ*, 357, 188
- Lucy, L. B. & Sweeney, M. A. 1971, *AJ*, 76, 544
- Maas, T., Van Winckel, H., & Waelkens, C. 2002, *A&A*, 386, 504
- Martinez, P., Kilkenny, D. M., Cox, G., et al. 2002, *Monthly Notes of the Astronomical Society of South Africa*, 61, 102
- Mathis, J. S. & Lamers, H. J. G. L. M. 1992, *A&A*, 259, L39
- Menzies, J. W., Cousins, A. W. J., Banfield, R. M., & Laing, J. D. 1989, *South African Astronomical Observatory Circular*, 13, 1
- Molster, F. J., Waters, L. B. F. M., Trams, N. R., et al. 1999, *A&A*, 350, 163
- Nyman, L.-A., Booth, R. S., Carlstrom, U., et al. 1992, *A&AS*, 93, 121
- Olson, F. M., Raimond, E., Neugebauer, G., et al. 1986, *A&AS*, 65, 607
- Olofsson, H., Eriksson, K., Gustafsson, B., & Carlstrom, U. 1993, *ApJS*, 87, 267
- Pols, O., Karakas, A., & Lattanzio, J. T. C. 2003, in *Symbiotic stars probing stellar evolution*, ed. M. Hack, in press
- Preston, G. W., Krzeminski, W., Smak, J., & Williams, J. A. 1963, *ApJ*, 137, 401
- Queloz, D., Casse, M., & Mayor, M. 1999, in *ASP Conf. Ser. 185: IAU Colloq. 170: Precise Stellar Radial Velocities*, ed. J. B. Hearnshaw & C. D. Scarfe, 13–+
- Raveendran, A. V. 1989, *MNRAS*, 238, 945
- Sargent, W. L. W. & Osmer, P. S. 1969, in *Mass Loss from Stars, Proceedings of the second Trieste Colloquium on Astrophysics*, ed. M. Hack, 57–+
- Shenton, M., Evans, A., & Williams, P. M. 1995, *MNRAS*, 273, 906
- Stellingwerf, R. F. 1978, *ApJ*, 224, 953
- van der Veen, W. E. C. J., Waters, L. B. F. M., Trams, N. R., & Matthews, H. E. 1994, *A&A*, 285, 551
- Van Winckel, H. 2001, *Ap&SS*, 275, 159
- . 2003, *ARA&A*, 1, in press
- Van Winckel, H. & Reyniers, M. 2000, *A&A*, 354, 135
- Van Winckel, H., Waelkens, C., Fernie, J. D., & Waters, L. B. F. M. 1999, *A&A*, 343, 202
- Van Winckel, H., Waelkens, C., & Waters, L. B. F. M. 1995, *A&A*, 293, L25
- Van Winckel, H., Waelkens, C., Waters, L. B. F. M., et al. 1998, *A&A*, 336, L17
- Waelkens, C., Van Winckel, H., Waters, L. B. F. M., & Bakker, E. J. 1996, *A&A*, 314, L17
- Waters, L., Waelkens, C., & Van Wickel, H. 1997, in *IAU Symp. 180: Planetary Nebulae*, ed. H. Habing & H. Lamers, Vol. 180, 313–+
- Waters, L. B. F. M., Cami, J., de Jong, T., et al. 1998, *Nat*, 391, 868
- Waters, L. B. F. M., Trams, N. R., & Waelkens, C. 1992, *A&A*, 262, L37
- Waters, L. B. F. M., Waelkens, C., Mayor, M., & Trams, N. R. 1993, *A&A*, 269, 242

Fig. 9. CO data : upper panel : low resolution CO(2-1) spectrum taken on 2/10/99, second panel : low resolution CO(2-1) spectrum taken on 28/07/00, third panel : total averaged of 5 spectra of the high resolution CO(2-1) line , bottom panel : total averaged spectrum of the low resolution CO(1-0) line. All velocities are heliocentric.

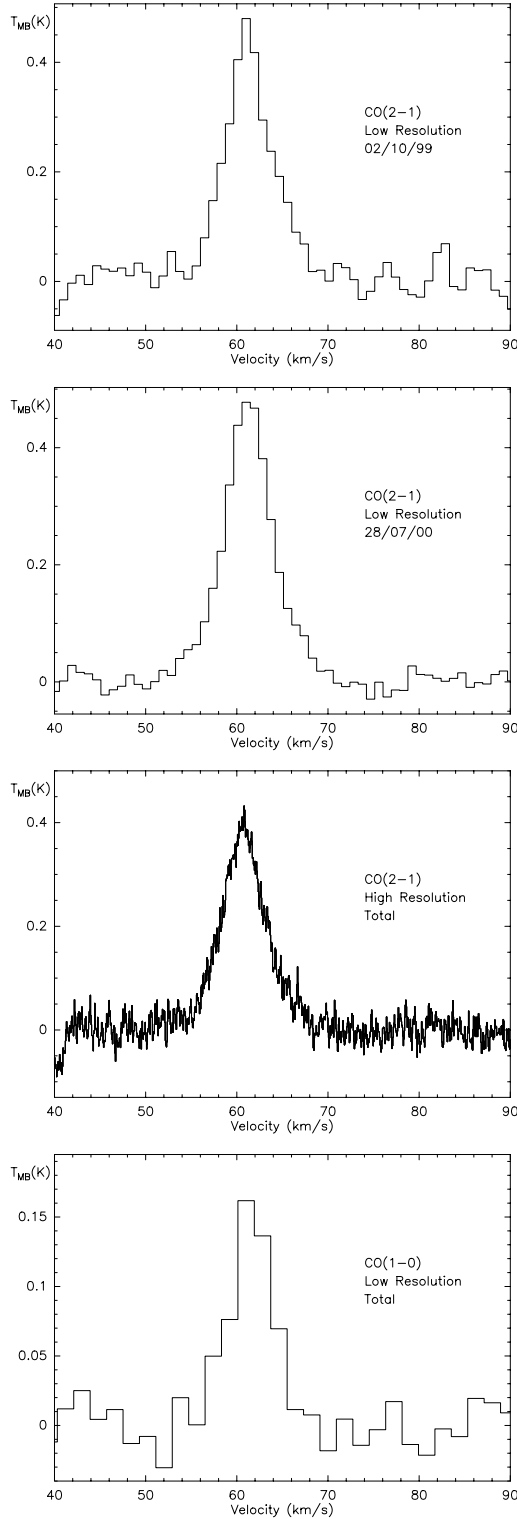


Fig. 10. The map of the environment of IRAS 08544 in low resolution CO(2-1).

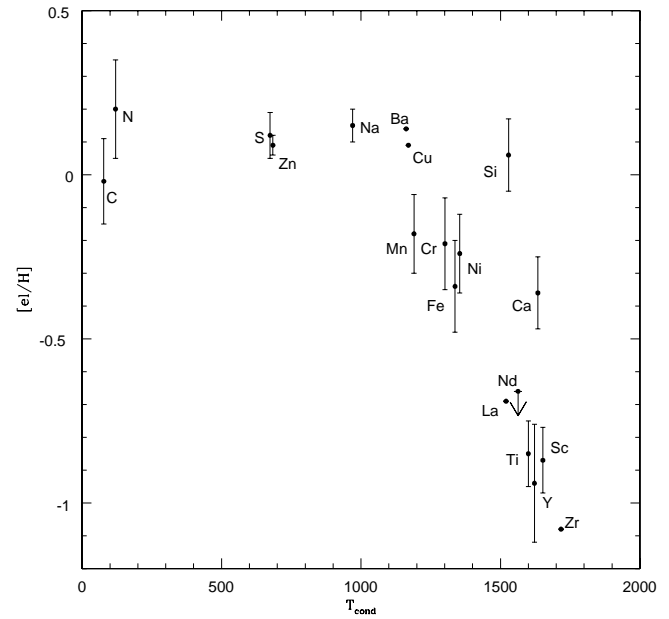
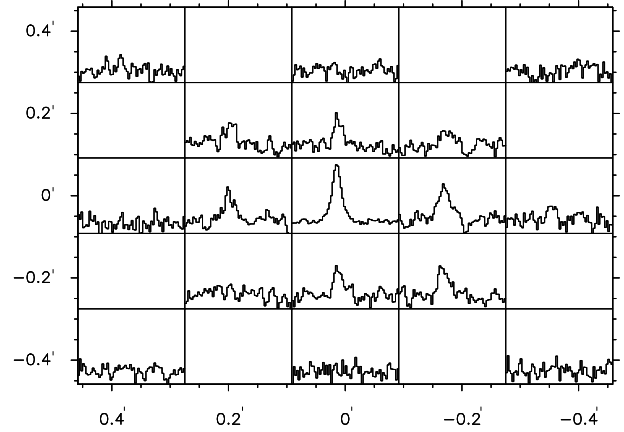


Fig. 11. The composition of IRAS 08544 against the dust condensation temperature of the chemical element.

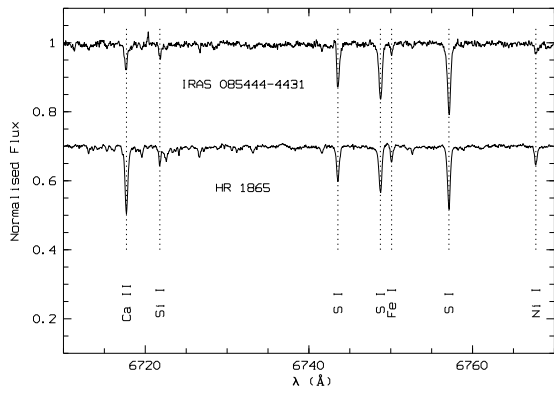


Fig. 12. Sample spectra of IRAS 08544 and HR 1865. The spectra are velocity corrected. HR 1865 is a massive supergiant with the same atmospheric parameters. All lines in HR 1865 are stronger than in IRAS 08544 except for the lines of S.

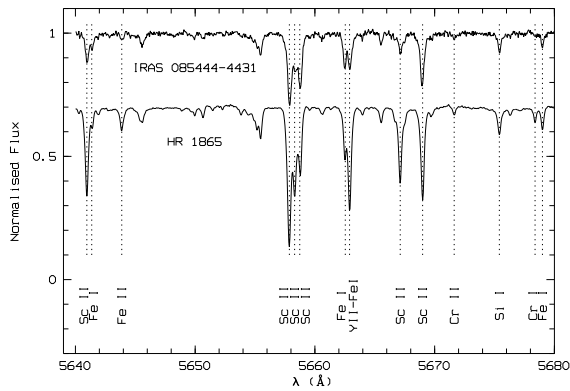


Fig. 13. Spectrum of IRAS 08544 around 5660 Å. All lines in HR 1865 are stronger than in IRAS 08544, but the difference in Sc-lines is largest.